Multivalent "attacker and guard" strategy for targeting surfaces with low receptor density

Document Version:
Publisher's PDF, also known as Version of Record (includes final page, issue and volume numbers)

Please check the document version of this publication:

• A submitted manuscript is the version of the article upon submission and before peer-review. There can be important differences between the submitted version and the official published version of record. People interested in the research are advised to contact the author for the final version of the publication, or visit the DOI to the publisher's website.
• The final author version and the galley proof are versions of the publication after peer review.
• The final published version features the final layout of the paper including the volume, issue and page numbers.

[Link to publication](#)

Nicholas B. Tito (iD)

View Online   Export Citation   CrossMark

The Journal of Chemical Physics

AIP Publishing

Multivalent "attacker and guard" strategy for targeting surfaces with low receptor density

View Online   Export Citation   CrossMark

Nicholas B. Tito[a] iD

AFFILIATIONS

Department of Applied Physics, Eindhoven University of Technology, P.O. Box 513, 5600 MB, Eindhoven,
The Netherlands and Institute for Complex Molecular Systems, Eindhoven University of Technology,
P.O. Box 513, 5600 MB, Eindhoven, The Netherlands

[a]Electronic mail: nicholas.b.tito@gmail.com

ABSTRACT

Multivalent particles, i.e., microscopic constructs having multiple ligands, can be used to target surfaces selectively depending on their receptor density. Typically, there is a sharp onset of multivalent binding as the receptor density exceeds a given threshold. However, the opposite case, selectively binding to surfaces with a receptor density below a given threshold, is much harder. Here, we present a simple strategy for selectively targeting a surface with a *low* density of receptors, within a system also having a surface with a higher density of the same receptors. Our strategy exploits competitive adsorption of two species. The first species, called "guards," are receptor-sized monovalent particles designed to occupy the high-density surface at equilibrium, while the second multivalent "attacker" species outcompetes the guards for binding onto the low-density surface. Surprisingly, the recipe for attackers and guards yields more selective binding with stronger ligand-receptor association constants, in contrast to standard multivalency. We derive explicit expressions for the attacker and guard molecular design parameters and concentrations, optimized within bounds of what is experimentally accessible, thereby facilitating implementation of the proposed approach.

Published under license by AIP Publishing. https://doi.org/10.1063/1.5086277

I. INTRODUCTION

Multivalency is a microscopic design strategy for targeting particles with two or more binding units ("ligands") to a target, such as a surface, having complementary binding units ("receptors").[1–8] Nature has exploited multivalency to define interaction paradigms at and between cell surfaces[1–3,9–22] and in the design of bacteria, viruses, and biomolecules themselves.[23–26] As a result, a large body of research to date has been dedicated to targeting surfaces of cells, cancerous tumors, and other microscopic objects via bio-inspired multivalent interactions.[14,15,25–44] Multivalency is also employed to design eloquent self-assembly pathways for synthetic ligand-coated nano- and colloidal particles, often utilizing DNA as their binding moieties due to their tunable hybridization free energy.[6,7,36,45–68] Due to the fact that multiple ligand-receptor bonds are involved in

multivalent interactions, their binding kinetics are nontrivial and can complicate the road to reaching equilibrium.[18,31,59,62,69,70]

The binding affinity of a multivalent particle depends strongly on the number of ligands it has and the receptor density of the target surface.[5,6,71] This is because the binding free energy between the two entities contains a nontrivial entropy term, whose magnitude depends on the number of ligands and receptors. One result of this is superselectivity, where the logarithm of the number of surface-bound particles increases super-linearly with the log of the surface receptor concentration.[5] The selectivity becomes larger for particles with more ligands and when the per-ligand binding energy becomes smaller. Therefore, high-valence particles with weak-binding ligands exhibit sharper surface binding transitions than low-valence particles with strong-binding ligands. This can be used to design multivalent particles that strongly bind to surfaces with many receptors,

while having little affinity for surfaces with even a slightly lower density of the same receptors.

A single species of multivalent particles cannot address the opposite scenario, namely, targeting a low-receptor-density surface but not one with a higher receptor density. This is because the entropy of binding—the contribution arising from ligand-receptor bonding permutations—always becomes more favorable for a multivalent particle as the surface receptor density increases. Therefore, particles that bind to a surface with few receptors will necessarily bind to one with many. To selectively target only a low receptor density surface, a different approach is needed.

By separately tuning the entropy and energy of binding, mixtures of different kinds of multivalent particles can exhibit "switch-like" surface binding.[72] For example, an equimolar mixture of low-valence nanoparticles with strong-binding ligands can compete with a high-valence weak-ligand species. Both nanoparticle species have the same core size and exclude the same area when bound to the surface. When the surface receptor density is low, the low-valence species selectively binds to the surface. Upon increasing the receptor concentration, there is a switch-point, after which the surface becomes occupied by the high-valence species. The surface receptor density thus acts to shift the balance between the entropic and energetic terms in the free energy of binding for the two species. The binding free energy of the low-valence strong-binding species is dominated by the energetic term; on the other hand, the high-valence weak-binding species has a substantial entropy of binding.

The present work takes this as inspiration and devises an "attacker and guard" strategy for selectively targeting a surface with low receptor density within a system that also has a surface with a higher density of the same receptors. This might be, for example, two populations of cells in a suspension, with one population having a high membrane concentration of a particular receptor and the other having a low concentration of the same receptors.

The strategy we propose entails using one species of particles, called "guards," to occupy the receptors on the high-density surface. These particles have a size on the order of a single receptor. A second larger species of particles, called "attackers," are then designed to out-compete the guards for binding on the low-receptor-density surface at equilibrium but not on the high-density surface. Experimental accessibility and robustness are emphasized in devising this recipe. The strategy may prove useful for selectively imaging cell surfaces *in vitro* that have globally or locally low receptor density, e.g., by making the attackers fluorescently active and the guards not via a DNA Points Accumulation for Imaging in Nanoscale Topography (DNA-PAINT) approach.[73] This approach may also have use in selective sequestration or aggregation of microscopic entities with a low receptor density, in which the attackers act as the aggregating agents.

II. TUNING MULTIVALENT BINDING BY MICROSCOPIC CONSTRUCTION

To begin, we briefly review how the binding free energy of a multivalent particle dictates its affinity to binding to a surface, as a function of the target surface's receptor density. This is important for understanding how to manipulate the binding affinity of two competing species for the more complex case of targeting a low-receptor-density surface.

The binding free energy of a multivalent particle is given by the standard relation $\beta G(N_R) = -\ln Q(N_R) - \ln z$, where Q is the partition function for the particle when it is adjacent to the receptor surface, and z is the fugacity of the particles in solution above the receptor surface. The quantity N_R is the number of receptors that are accessible to the particle when it is adjacent to the surface. This is defined as $N_R = \sigma_R a^2$, where σ_R is the number of receptors per unit area on the surface (the "receptor density") and a is the diameter of the multivalent particle and its ligands. We refer to one a^2-sized area element of the receptor surface as a surface "lattice site."

Multivalent particles at low concentration can be assumed to follow ideal gas statistics, in which the fugacity z is related to the molar concentration "$[C]$" of the particles in solution by

$$[C] = \frac{z}{N_A v_{ex}}. \tag{1}$$

Here, N_A is Avogadro's number, and v_{ex} is the excluded volume (or "localization volume") for one multivalent particle. Note that v_{ex} must be in units of decimeters[3] in order for the concentration $[C]$ to be in the appropriate units of moles/liter.

When a multivalent particle is adjacent to a binding surface, it can have one or more additional "nonspecific" (i.e., nonmultivalent) interaction free energy contributions. Collecting all of these additional contributions into the quantity "G_{NS}," then the total binding free energy of the multivalent particle is

$$\beta G(N_R) = -\ln Q(N_R) - \ln z + \beta G_{NS}. \tag{2}$$

Written this way, *the partition function $Q(N_R)$ explicitly contains only the "multivalent" ligand/receptor bonding contributions to the binding free energy.* Unless otherwise noted, we henceforth set βG_{NS} to zero and focus attention on the multivalent binding contributions in $Q(N_R)$.

When receptors are immobile and *uniformly* placed on the surface at a density of σ_R, the partition function $Q(N_R)$ for a lattice site when occupied by a multivalent particle is well described[5,19] by

$$Q(N_R) = \sum_{\lambda=0}^{N^*} \binom{N_R}{\lambda}\binom{N_L}{\lambda}\lambda! e^{-\beta\lambda f}, \tag{3}$$

where f is the free energy for forming a single ligand-receptor bond, N_L is the effective number of ligands on the multivalent particle that can access the surface for receptor binding at any given time, and $N^* = \min(N_R, N_L)$. This expression effectively treats the receptors and ligands as an ideal gas within the surface lattice site, while crucially enforcing that they each may only have zero or one binding partner in any given microstate. Note that the effective valence N_L is almost always less than the total number of ligands on the particle. This is because not all ligands can simultaneously reach the receptor surface for binding, depending on how the multivalent particle is oriented. For multivalent constructs, it is the "effective" valence that dictates binding behaviour, and this is what the quantity N_L signifies throughout our discussion.

Adding in Poisson fluctuations to the number of receptors in each lattice site considerably simplifies Eq. (3). With a Poisson distribution centered around a mean value of N_R receptors per lattice site, the probability the multivalent particle "sees" j receptors within area a^2 follows $P(j; N_R) = e^{-N_R}N_R^j/j!$. In this case, Eq. (3)

simplifies to[19]

$$Q(N_R) = \left(1 + N_R e^{-\beta f}\right)^{N_L}. \qquad (4)$$

Strictly speaking, this form is only exact when the coverage of bound multivalent particles on the receptor surface is low, such that each bound particle can independently sample the Poisson distribution of receptors. For higher surface coverage, the adsorption statistics become multi-Langmuir, and this must be calculated numerically (see Ref. 74 for a mathematical and experimental discussion of this regime). To proceed analytically for the present discussion, we adopt Eq. (4) and then remark on potential discrepancies compared to the more exact multi-Langmuir adsorption later on in the discussion. Note that Eq. (4) is also exact when the receptors are mobile on the surface, nondepletable (i.e., coming from a grand canonical reservoir), and at an average concentration of N_R per lattice site. However, for the present study, we assume that the receptors are immobile over the time scale of multivalent particle binding and equilibration.

Given $Q(N_R)$ in Eq. (4), the binding free energy for a multivalent particle is

$$\beta G(N_R) = -N_L \ln\left(1 + N_R e^{-\beta f}\right) - \ln z + \beta G_{NS}. \qquad (5)$$

The probability that a surface lattice site is occupied by a multivalent particle is then

$$P_b(N_R) = \frac{e^{-\beta G(N_R)}}{1 + e^{-\beta G(N_R)}}. \qquad (6)$$
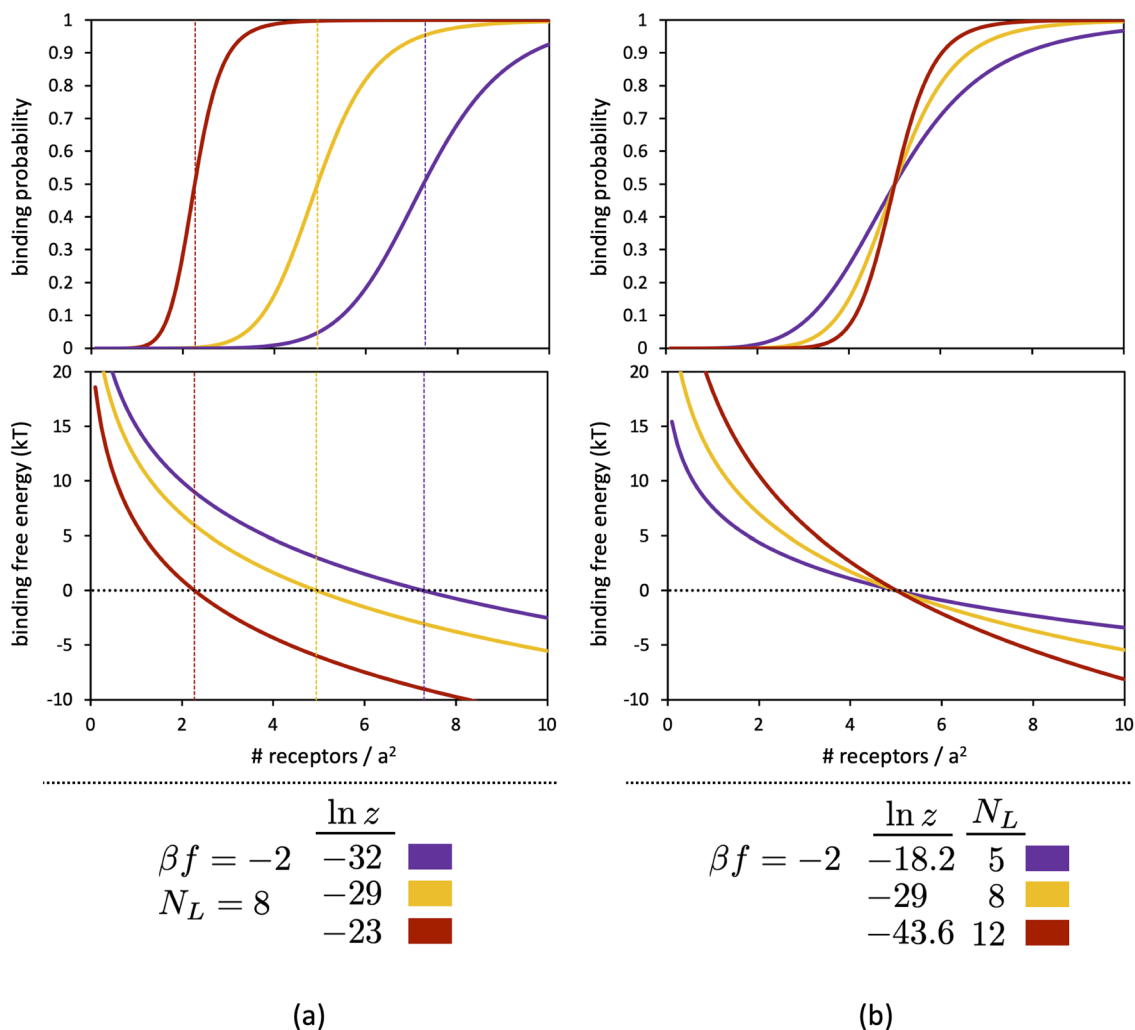
FIG. 1. Multivalent binding probability [Eq. (6)] (upper panels) and binding free energy (lower panels) as a function of the number of receptors N_R per surface lattice site of size a^2. In (a), the ligand-receptor binding free energy $\beta f = -2$ and number of ligands $N_L = 8$ are kept fixed, while the fugacity of the particles is set to $\ln z = -32$, -29, and -23 (purple, yellow, and red). Vertical dashed lines indicate inflection points for each adsorption profile. In (b), the particle ligand-receptor binding free energy is also fixed at $\beta f = -2$, while the number of ligands on the particle is set to $N_L = 5$, 8, and 12 (purple, yellow, and red). In each case, the fugacity is adjusted such that the binding transition occurs at $N_R = 5$.

When $\beta G(N_R)$ is greater than zero (i.e., an unfavorable binding free energy change), then $P_b(N_R)$ goes to zero. Similarly, when $\beta G(N_R)$ is less than zero, corresponding to a favorable free energy of binding, then $P_b(N_R)$ goes to unity. Thus, $\beta G(N_R) = 0$ corresponds to the binding transition, and the derivative of $\beta G(N_R)$ with respect to N_R at $\beta G(N_R) = 0$ reflects the sharpness of the transition.

Equation (5) shows us how the multivalent binding free energy changes with N_R, f, N_L, z, and βG_{NS}. The fugacity z ($\propto$ concentration $[C]$) shifts the binding free energy $\beta G(N_R)$ up or down by a constant. It therefore provides a convenient handle for adjusting the receptor density σ_R at which the adsorption transition occurs. This is illustrated in Fig. 1(a). As the fugacity grows smaller, then the overall binding free energy shifts higher (more unfavorable). The receptor density σ_R where the adsorption transition occurs correspondingly increases, and the sharpness of the transition decreases [as the local derivative of $\beta G(N_R)$ for increasing N_R gets smaller].

The sharpness of the binding transition can be tuned by adjusting the molecular construction of the multivalent particle, via its valence N_L and ligand-receptor binding strength f. Figure 1(b) shows examples of tuning the adsorption sharpness by changing N_L. In each case, the fugacity has been tuned so that the adsorption transition is centered at $N_R = 5$. Making N_L larger causes the gradient of $\beta G(N_R)$ with N_R to be steeper and more negative, leading to a sharper binding transition.

The free energy curves in Figs. 1(a) and 1(b) can also be vertically shifted by altering the "nonspecific" binding free energy βG_{NS}. The quoted values of $\ln z$ in those examples can, for example, be equivalently interpreted as "effective" fugacities given by $\ln z_{true} - \beta G_{NS}$, where the former is the true solution fugacity determined by the multivalent particle concentration. Since βG_{NS} can also be tuned by the chemical design, in principle, then it is an additional adjustment knob for *uniformly* shifting the multivalent binding free energy if tuning the particle concentration proves to be impractical. (An example would be a particular target receptor surface that requires a vanishingly small or infeasibly large bulk solution concentration of multivalent particles in order to reach a desired binding equilibrium.)

III. TARGETING A LOW-RECEPTOR-DENSITY SURFACE WITH TWO COMPETING SPECIES

The binding free energy of a multivalent particle, $\beta G(N_R)$, can be completely tailored by the parameters f, N_L, and z. This can be used to design a multivalent species that binds strongly to a surface with a high receptor density while not binding to one with a lower density. However, it is impossible to achieve the opposite case with just one multivalent binder. As is apparent in Figs. 1(a) and 1(b), the binding free energy cannot be manipulated in such a way that the multivalent particle only binds at low surface receptor concentration.

To solve this problem, we can introduce a second particle species that competes for surface binding with the original species. The goal is to define the second species such that it blocks the first from binding to the high-receptor-density surface but not the low-density surface. We call this second species the "guards," and the original species the "attackers." The forthcoming "Attacker and Guard" strategy is graphically depicted in Fig. 2, showing the molecular ingredients, salient mathematical parameters, and intended

equilibrium distribution of attackers and guards on the two receptor surfaces.

To start, the guards are defined to be a roughly *receptor-sized monovalent* species. The free energy of binding for a monovalent species is *independent* of the surface receptor density. Each receptor has a partition function of the form

$$q_{receptor} = 1 + z_{guard}e^{-\beta f_{guard}}, \tag{7}$$

where f_{guard} is the free energy for forming a guard-receptor bond and z_{guard} is the guard fugacity. The first term in $q_{receptor}$ is the weight for when the receptor is not bound to anything, and the second is for when it is bound to a guard particle. The free energy of a single receptor is then just $-\ln(q_{receptor})$.

However, to compare the guard binding free energy to the attackers, we must consider the total free energy of guard binding over the full area a^2 occupied by an attacker. This quantity depends *linearly* on the number N_R of receptors within a^2

$$\beta G_{guard}(N_R) = -\ln\left(q_{receptor}^{N_R}\right) = -N_R \ln\left(1 + z_{guard}e^{-\beta f_{guard}}\right)$$
$$= -N_R C_{guard}. \tag{8}$$

Here, the combined tunable guard parameter

$$C_{guard} \equiv \ln\left(1 + z_{guard}e^{-\beta f_{guard}}\right) \tag{9}$$

has been defined for notational clarity in subsequent equations.

On the other hand, the free energy of the lattice site when occupied by an attacker depends *logarithmically* on N_R in the lattice site, via Eq. (5),

$$\beta G_{attacker}(N_R) = -N_L \ln\left(1 + N_R e^{-\beta f_{attacker}}\right) - \ln z_{attacker}, \tag{10}$$

assuming no nonspecific binding free energy contribution βG_{NS}. Importantly, we assume that *when an attacker is bound, it excludes all receptors over the area a^2 from binding to any guards.* This assumption is most likely to hold when the attacker is a solid structure like, e.g., a ligand-coated nanoparticle, vesicle, or virus. The implications of this assumption breaking down are examined later.

The different scaling of the attacker and guard binding free energies (per lattice site) with N_R can be exploited, as shown in Fig. 3(a). In this example, we suppose that the low-density surface has $N_R = 4 \equiv N_R'$, and the high-density surface has $N_R = 10 \equiv N_R''$. The blue curve in Fig. 3(a) plots $\beta G_{guard}(N_R)$ as a function of N_R. The slope of the line is controlled by the guard fugacity z_{guard} and binding strength f_{guard}. The red curve in Fig. 3(a) displays $\beta G_{attacker}(N_R)$. The weaker logarithmic dependence of $\beta G_{attacker}(N_R)$ on N_R has been exploited to tune the attacker's design (via N_L, $f_{attacker}$, $z_{attacker}$) such that: at N_R', $\beta G_{attacker}(N_R')$ $< \beta G_{guard}(N_R')$; while at N_R'', $\beta G_{guard}(N_R'') < \beta G_{attacker}(N_R'')$.

The resulting binding behavior of the attackers and guards is displayed in Fig. 3(b). The probability that a surface site is occupied by an attacker is

$$P_b^{attacker}(N_R) = \frac{e^{-\beta \Delta G(N_R)}}{1 + e^{-\beta \Delta G(N_R)}}, \tag{11}$$

where
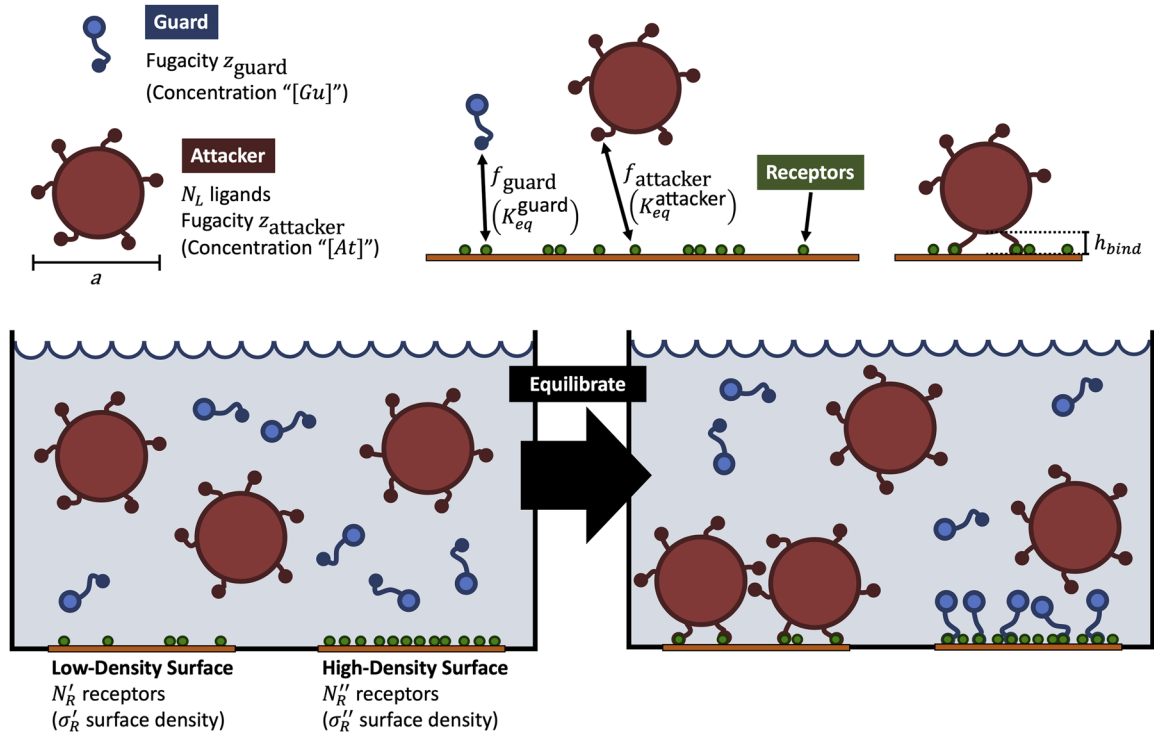
FIG. 2. Graphical depiction of the "Attacker and Guard" targeting strategy, showing key ingredients, mathematical parameters, and sought-after equilibrium binding distribution of particles. Upper half of image shows attackers, guards, and a receptor surface, along with relevant mathematical parameters (described in main text). Lower half of image shows attackers and guards in a hypothetical solution containing a low- and high-receptor-density surface. On the left, attackers and guards have just been added, while on the right, equilibrium has been reached.
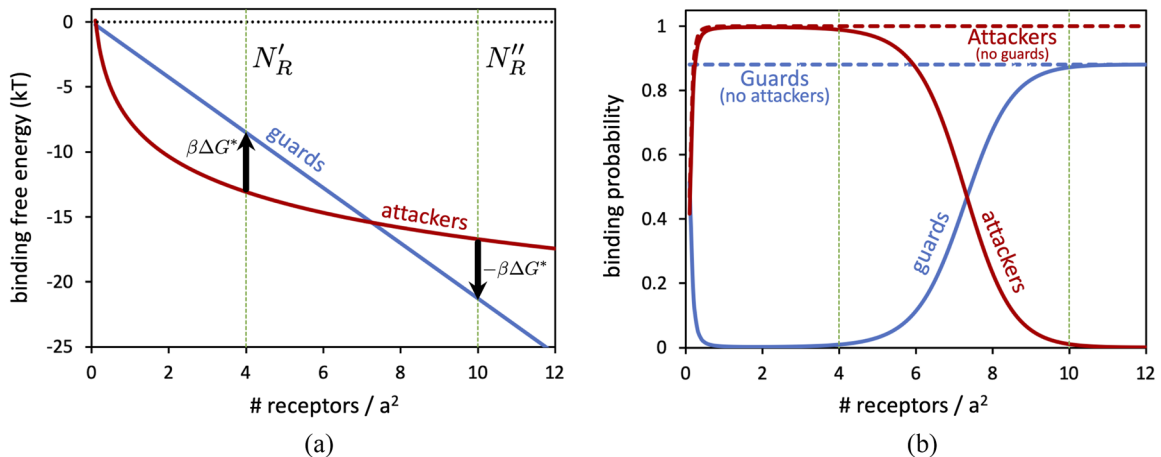
FIG. 3. Binding free energy [(a), via Eqs. (8) and (10)] and surface adsorption probability [(b), via Eqs. (11) and (13)] for attackers (red curves) and guards (blue curves) as a function of the average number of receptors per surface lattice site of area a^2. Green vertical lines indicate the low-receptor-density and high-receptor-density surfaces, with $N_R' = 4$ and $N_R'' = 10$, respectively. In (b), solid lines are for when attackers and guards coexist in the same system, while dashed lines are for when they are separately in the system. Multivalent attacker parameters are $N_L = 4$, $\beta f_{attacker} = -3$, and $\ln z_{attacker} = -4.53$, while monovalent guard parameters are $\beta f_{guard} = -4$ and $\ln z_{guard} = -2$. Attacker fugacity $z_{attacker}$ has been chosen such that $\beta \Delta G(N_R') = -\beta \Delta G(N_R'')$, indicated as $\beta \Delta G^*$ in (a) here.

$$\beta\Delta G(N_R) \equiv \beta G_{\text{attacker}}(N_R) - \beta G_{\text{guard}}(N_R). \quad (12)$$

For comparison, we also plot the probability that a single receptor is attached to a guard

$$P_b^{\text{guard}}(N_R) = \left(\frac{z_{\text{guard}} e^{-\beta f_{\text{guard}}}}{1 + z_{\text{guard}} e^{-\beta f_{\text{guard}}}} \right) \left(1 - P_b^{\text{attacker}}(N_R) \right). \quad (13)$$

These are derived in Appendix A.

In Fig. 3, the guard and attacker fugacities have been set to $\ln z_{\text{guard}} = -2$ and $\ln z_{\text{attacker}} = -4.53$. Using Eq. (1), a rough feasibility check can be made for the molar concentrations these fugacities correspond to assuming that there is no nonspecific binding free energy (βG_{NS}) contribution. For example, considering "receptor-sized" guards of length 10 nm (≈ 1 hemagglutinin unit on the exterior of an influenza virus particle), and attackers of size 100 nm, then these fugacities correspond to guard and attacker concentrations of around $[Gu] \approx 200~\mu M$ and $[At] \approx 18$ nM. These concentrations, along with the choices of $\beta f_{\text{guard}} = -4$, $N_L = 4$, and $\beta f_{\text{attacker}} = -3$ in that figure, are well within accessible experimental range.

At N_R', the attackers are strongly bound, while at N_R'', the guards outcompete the attackers for binding. The value of N_R where $\beta G_{\text{guard}}(N_R) = \beta G_{\text{attacker}}(N_R)$ defines the "switch point" between the two species. Combining both species into the same system is essential, as alone, one or the other species would strongly bind to both the low- and high-density surfaces [dashed blue and red lines in Fig. 3(a)].

The effectiveness of the targeting recipe is assessed by the difference in attacker binding probabilities at N_R' and N_R'', defined as

$$\text{Effectiveness} \equiv \phi \equiv P_b^{\text{attacker}}(N_R') - P_b^{\text{attacker}}(N_R''). \quad (14)$$

Values of ϕ near unity are optimal, 0 means that the attackers bind equally well to N_R' and N_R'', while negative values (approaching -1) mean that the attackers favor binding to N_R'' rather than N_R'.

In order to achieve an effectiveness ϕ of unity, the attacker/guard binding free energy difference $\beta\Delta G(N_R)$ must go to negative infinity at N_R' and positive infinity at N_R''. Therefore, to proceed further, we seek the attacker and guard design parameters that lead to a given *chosen* effectiveness ϕ.

By inspection of Fig. 3(a), the maximum possible effectiveness of an attacker+guard design is set by the slope of the guard free energy (blue line) as a function of N_R. The larger and more negative the slope, the larger the free energy difference between N_R' and N_R''. The connection between a desired ϕ and the necessary C_{guard} is developed in Sec. IV.

The remaining task is to find an optimal attacker design, i.e., N_L, z_{attacker}, and f_{attacker}. The best attacker design is one in which their free energy of binding (red curve) as a function of N_R is nearly constant between N_R' and N_R'' so as to bisect the blue guard curve in this interval in Fig. 3(a). Doing so obtains the most negative $\beta\Delta G(N_R')$ and most positive $\beta\Delta G(N_R'')$. Based on Eq. (10), this occurs when the attacker has *few strong-binding* ligands.

The number of ligands N_L and ligand/receptor bonding strength f_{attacker} of the attackers are set by the chemical design. Supposing these are predefined for the time being, we then seek the attacker fugacity (concentration) z_{attacker} that maximizes the

targeting effectiveness ϕ. Attackers can be readily titrated into a system so that the level of control over z_{attacker} is very high compared to the molecular design. It is therefore a convenient experimental control parameter to optimize over for the attackers.

The attacker fugacity z_{attacker} that maximizes the targeting effectiveness is where

$$\frac{d\phi}{d\ln z_{\text{attacker}}} = 0. \quad (15)$$

This is carried out in Appendix B, where we find that the largest effectiveness is obtained by choosing z_{attacker} such that

$$\beta\Delta G(N_R') = -\beta\Delta G(N_R''). \quad (16)$$

We call this optimum "$\beta\Delta G^*$": A free energy "gap" that is directly tuned by the design of the guards and attackers. Inserting the condition in Eq. (16) into Eq. (14) yields

$$\text{Optimal Effectiveness} \equiv \phi^* = \frac{e^{-\beta\Delta G^*} - 1}{e^{-\beta\Delta G^*} + 1}. \quad (17)$$

Tuning of the attacker fugacity to satisfy this optimum condition has been carried out in Fig. 3(a), and the symmetric free energy gap $\beta\Delta G^*$ is indicated. The "tolerance" of the targeting design is quantified by the width of the optimum in targeting effectiveness at $\beta\Delta G(N_R') = -\beta\Delta G(N_R'') = \beta\Delta G^*$,

$$\text{Design Tolerance for } \phi^* \equiv -\left(\frac{d^2\phi}{[d\ln z_{\text{attacker}}]^2} \right)^{-1} \approx \frac{1}{2} e^{-\beta\Delta G^*}. \quad (18)$$

Equations (17) and (18) indicate that *the most effective and most tolerant targeting design is obtained when the free energy gap $\beta\Delta G^*$ is large and negative.*

IV. OPTIMAL DESIGN OF ATTACKERS AND GUARDS

The quantity $\beta\Delta G^*$ is directly tuned by the molecular design of the attackers and guards. The necessary $\beta\Delta G^*$ in order to achieve a given effectiveness ϕ^* is obtained by inverting Eq. (17), yielding $\beta\Delta G_{\text{needed}}^* = -\ln\left(\frac{1+\phi^*}{1-\phi^*} \right)$. The free energy gap in terms of the attacker and guard binding free energies is $\beta\Delta G^* = \beta G_{\text{attacker}}(N_R') - \beta G_{\text{guard}}(N_R')$, subject to the constraint $\beta G_{\text{attacker}}(N_R') - \beta G_{\text{guard}}(N_R') = \beta G_{\text{guard}}(N_R'') - \beta G_{\text{attacker}}(N_R'')$ given by Eq. (16).

These three relations, applied to the guard and attacker binding free energies [Eqs. (8) and (10)], result in closed-form expressions for the necessary attacker and guard solution concentrations $[At]^*$ and $[Gu]^*$ to achieve a desired targeting effectiveness ϕ^*. The derivation is carried out in Appendix C, resulting in

$$[At]^* = \frac{1}{N_A h_{\text{bind}} a^2} \frac{\left[\left(\frac{q_L(c_R'')}{q_L(c_R')} \right)^{\frac{N_L}{2}} \left(\frac{1+\phi^*}{1-\phi^*} \right) \right]^{\frac{c_R'' + c_R'}{c_R'' - c_R'}}}{\left[q_L(c_R') q_L(c_R'') \right]^{\frac{N_L}{2}}}, \quad (19)$$

$$[Gu]^* = \frac{1}{K_{eq}^{\text{guard}}} \left\{ \left[\left(\frac{q_L(c_R'')}{q_L(c_R')} \right)^{\frac{N_L}{2}} \left(\frac{1+\phi^*}{1-\phi^*} \right) \right]^{\frac{2}{N_A a^2(c_R'' - c_R')}} - 1 \right\}, \quad (20)$$

where $q_L(c_R')$ and $q_L(c_R'')$ are dimensionless quantities calculated by

$$q_L(c_R) = \left(1 + \frac{c_R K_{eq}^{\text{attacker}}}{h_{bind}}\right). \tag{21}$$

The expressions are presented here in the chemical equilibrium form, to facilitate experimental implementation. Appendix C details the mathematical transformations involved to translate the statistical mechanical theory into the form shown here.

The molar equilibrium association constants K_{eq}^{attacker} and K_{eq}^{guard} are for, respectively, binding between a free receptor and a single free ligand on the attacker and between a free receptor and a guard particle in solution. The quantities c_R' and c_R'' are "surface receptor molarities" (in units of moles of receptors per unit surface area) on the low- and high-density surfaces, respectively, and a is the diameter of the attacker (including its ligand corona). These are related to the previously employed surface densities σ_R by $c_R = \sigma_R/N_A$. The quantity h_{bind} is the equilibrium binding height of the attacker; its precise definition depends on the type of construct the attacker is to be discussed shortly. Finally, N_L is the number of ligands on the attacker species.

Equations (19) and (20) provide physical insight. As the desired effectiveness ϕ^* is increased to unity, then the required attacker and guard concentrations (or association constants) grow very large. Therefore, *the low-receptor density surface can be targeted more effectively when the attackers and guards have a larger overall binding affinity*. This is the opposite to standard one-component multivalent targeting of high-density surfaces, in which weak ligand-receptor bonds yield higher selectivity.

The remainder of this section takes a closer look at the guard and attacker parameters in Eqs. (19) and (20). The kinetics involved to reach binding equilibrium between the two competing adsorbers are illustrated, and a suggested "recipe" for adding attackers and guards that circumnavigates potential kinetic barriers is outlined. To finish, factors that enhance the tolerance of the design are discussed, while also remarking on effects not considered in our theory which might *reduce* the targeting effectiveness.

A. Equilibrium constants and attacker binding height in the context of experiment

The binding constant K_{eq}^{attacker} for the attacker ligands includes the enthalpic contribution to the ligand/receptor bond, as well as the extra (entropic) free energy cost $\Delta G_{\text{lig, cnf}}$ for bond formation. Usually in the experiment, the ligand/receptor binding constant is only measured for the case where the receptor and ligand structures are free in solution and untethered to any host surfaces. This reference ligand/receptor binding constant, "$K_{eq}^{\circ,\text{attacker}}$," is mapped to the binding constant for the ligands when attached to the attacker particle by

$$K_{eq}^{\text{attacker}} = K_{eq}^{\circ,\text{attacker}} e^{-\beta \Delta G_{\text{lig, cnf}}}. \tag{22}$$

Detailed discussions and models for approximating the extra entropic free energy penalty $\Delta G_{\text{lig, cnf}}$ for ligand/receptor binding are given in Refs. 6 and 8.

The quantity h_{bind} is a binding distance parameter. It controls the receptor "effective molarity" that the ligands on an attacker "see"

when the attacker is surface-bound.[19] Appendix C describes this in greater mathematical detail.

The choice of how to precisely define h_{bind} depends on the type of construct that the attacker is, as illustrated in Fig. 4. For example, if the attacker is a star polymer or dendrimer construct,[31] then h_{bind} should be taken to be the distance between the receptor surface and the center of the star. If the attacker is a solid particle-type construct like a DNA-coated nanoparticle or a surface-functionalized vesicle, then h_{bind} should be defined as the equilibrium distance between the outer surface of the attacker and the receptor surface.

In the latter case, whether or not h_{bind} should include the lengths of the receptors or ligands depends on how densely packed they are on their respective surfaces. For example, if the attacker has a dense packing of binding ligands (like, e.g., the influenza virus),
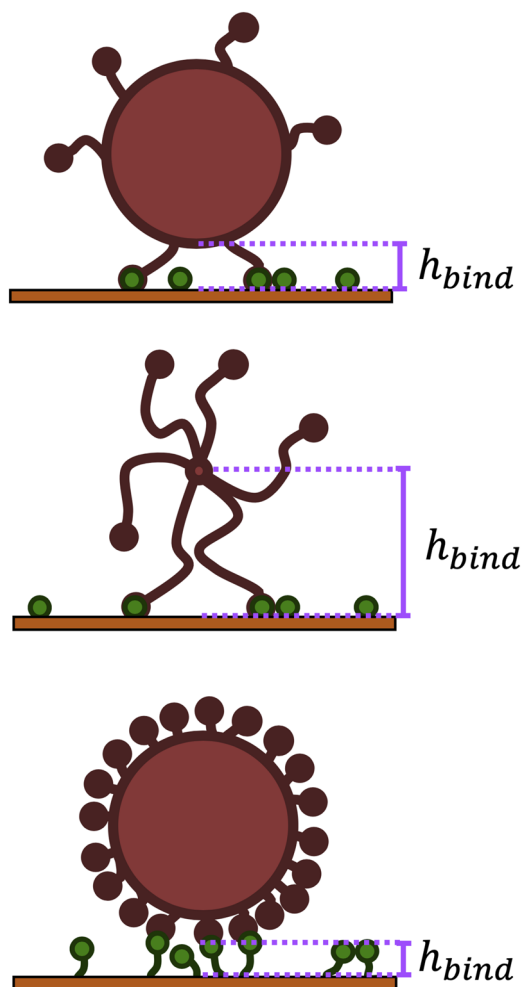
FIG. 4. Possible definitions for the equilibrium binding height parameter h_{bind}, depending on the multivalent attacker structure. Top image depicts a multivalent particle with a solid core and flexible ligands, interacting with a surface of short/inflexible receptors. Middle image is a star polymerlike structure or dendrimerlike structure interacting with short/inflexible receptors. Finally, the bottom image is a spherical structure with densely packed short/inflexbile ligands (e.g., like an influenza virus) interacting with flexible receptors.

then one could argue that h_{bind} should be measured from the exterior of the ligand corona to the receptor substrate. However, if the ligands are long and flexible or at a relatively low surface density, then h_{bind} is better defined as going all the way to the solid exterior of the attacker.

For purpose of demonstration, Fig. 5 shows experimentally relevant examples of how the optimal attacker and guard concentrations given by Eqs. (19) and (20) vary with choice of binding constants. The diameter of an attacker is set to $a = 50$ nm, with an equilibrium binding height $h_{bind} = 15$ nm. The low-receptor-density surface is chosen to have $\sigma'_R a^2 = 5$ receptors per attacker "footprint" and the high-density surface $\sigma''_R a^2 = 10$. The attacker particles are defined to have $N_L = 4$ ligands. Results have been calculated for three choices of desired targeting effectiveness ϕ^*.

In Eq. (20), we immediately see that the optimal guard concentration always scales with the binding constant K_{eq}^{guard} as
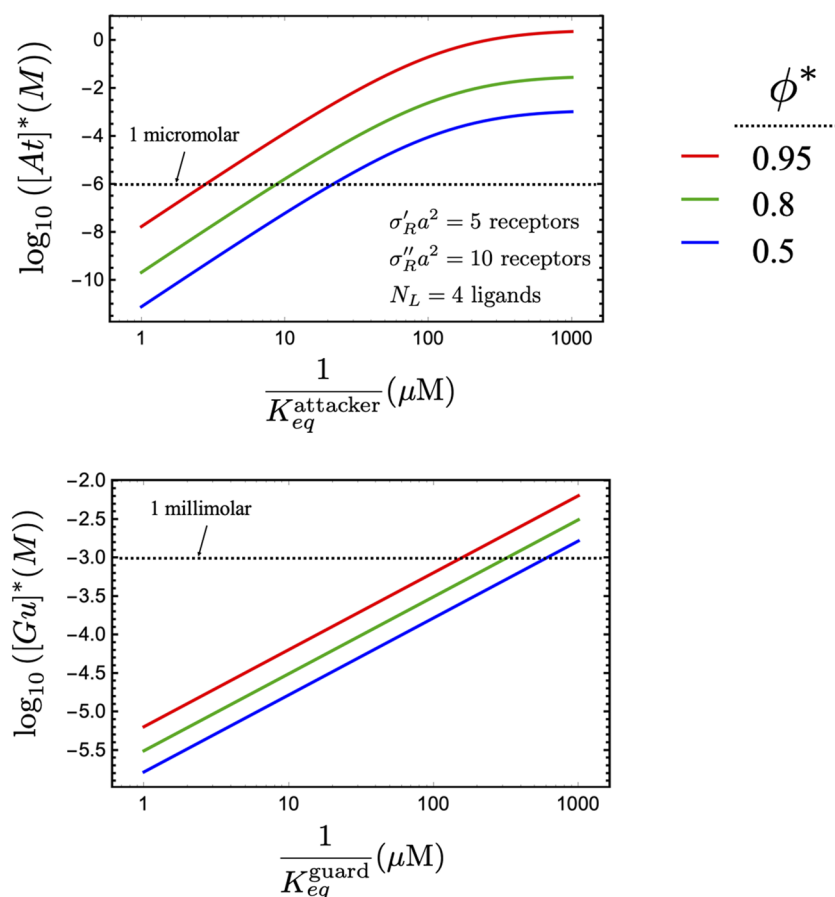
$$[Gu]^* \propto \frac{1}{K_{eq}^{guard}}.$$

The attackers behave in a more complex way. However, when the attacker ligands are strong-binding, then the ratio $(q_L(c''_R)/q_L(c'_R)) \rightarrow (c''_R/c'_R)$ in Eqs. (19) and (20). In this limit, the optimal attacker

concentration scales as

$$[At]^* \propto \left(\frac{1}{K_{eq}^{attacker}}\right)^{N_L}.$$

This scaling relation is noted in the upper panel of Fig. 5 when the attacker ligands are strong-binding. The logarithm of $[At]^*$ varies nearly linearly with the logarithm of the reciprocal ligand/receptor binding constant (i.e., the *dissociation* constant $K_d^{attacker}$) when $K_d^{attacker}$ is small. For relatively strong-binding ligands, where $K_d^{attacker}$ is around 1 μM, then the optimal solution concentration of attackers is in the micromolar to nanomolar range. Weakening the ligand/receptor $K_d^{attacker}$ brings $[At]^*$ to higher concentrations. Choosing a larger targeting effectiveness ϕ^* also acts to increase the optimal $[At]^*$ range.

The story for the guards is similar in the lower panel of Fig. 5. The scaling of $[Gu]^* \propto \frac{1}{K_{eq}^{guard}}$ is clear, although it is less steep than for the attackers, due to the lack of the exponent N_L on the (monovalent) guards. When the guard dissociation constant is around 1 μM, the optimal concentration is also in the micromolar range. Increasing the dissociation constant into the millimolar range accordingly brings the optimal guard concentration into that range as well.

FIG. 5. Logarithm of the optimal attacker (upper panel) and guard (lower panel) concentrations as a function of reciprocal binding constants $1/K_{eq}^{attacker}$ and $1/K_{eq}^{guard}$ (in units of micromolar). Results are calculated using Eqs. (19) and (20). Attackers are defined to have $N_L = 4$ ligands, a diameter of $a = 50$ nm, and an equilibrium binding height $h_{bind} = 15$ nm. The low- and high-receptor-density surfaces have $\sigma'_R a^2 = 5$ and $\sigma''_R a^2 = 10$ receptors per attacker footprint a^2, respectively. Calculations are displayed for three choices of targeting effectiveness $\phi^* = 0.95$, 0.8, and 0.5 (red, green, and blue). For guard calculations, attacker ligand/receptor binding constant is set to $1/K_{eq}^{attacker} = 10$ μM.

B. Kinetics on the road to equilibrium and suggested sequence of ingredients

Strong-binding attackers and guards have the limitation of long equilibration times since both species will have strong affinity for both receptor surfaces. The desired equilibrium binding distribution of attackers and guards shown in Fig. 3(b) may therefore take a very long time to achieve, as the unbinding rates of the attackers and guards on either surface decreases exponentially as the binding free energy grows larger and more negative (favourable).

For example, monovalent binders with a binding free energy of f (corresponding to an equilibrium association constant of K_{eq}) have an unbinding time scale that goes as the Arrhenius form

$$\frac{\tau_{\text{off}}^{\text{mono}}}{\tau^0} = e^{-\beta f} \propto K_{eq}, \qquad (23)$$

where τ^0 is a characteristic time scale. (This form assumes that there is no appreciable activation barrier to unbinding.) The unbinding time scale $\tau_{\text{off}}^{\text{mono}}$ grows longer for strong-binding (e.g., larger negative βf and larger K_{eq}) particles. For multivalent binders with ligand/receptor bonds of strength f_{LR}, the unbinding time scale increases exponentially with the average number $\bar{m}$ of bonds[31]

$$\frac{\tau_{\text{off}}^{\text{multi}}(\bar{m})}{\tau_{\text{LR}}^0} = \frac{e^{-\beta G_{NS}}}{\bar{m}} e^{-\beta \bar{m} f_{\text{LR}}} \propto \left(K_{eq}^{\text{LR}} \right)^{\bar{m}}, \qquad (24)$$

where τ_{LR}^0 is the time scale (reciprocal rate) of ligand/receptor association when both entities are free in solution at 1M reference concentration, and βG_{NS} contains all of the nonspecific interaction free energy contributions between the multivalent particle and the target surface as noted earlier in Eq. (2).

When the ligands on the attackers are strong-binding, as the present strategy calls for, then $\tau_{\text{off}}^{\text{multi}}(\bar{m})$ can potentially grow very long compared to $\tau_{\text{off}}^{\text{mono}}$ for the guards. To pre-emptively circumvent this kinetic barrier, we can envision the recipe depicted in Fig. 6 for reaching an attacker and guard binding equilibrium:

1. Add monovalent guards.
2. Equilibrate.
3. Add multivalent attackers.
4. Equilibrate again.

By this route, the only exchange necessary is on the low-receptor-density surface, where monovalent guards must unbind in order to allow the more favorably binding multivalent attackers to attach (Fig. 6, lower right). In the experimental design, the guard K_{eq}^{guard} can be chosen to be a strong-binding yet kinetically reasonable value, and then the concentration $[Gu]^*$ can be chosen via Eq. (20). The guard binding constant will therefore set the time scale τ_{off} that must be waited for the final equilibrium to be reached.

C. Making a more tolerant design

In Eq. (18), we found that the tolerance of the Attacker and Guard strategy grows exponentially larger by designing a larger (more negative) free energy gap $\beta\Delta G^*$. Let us now examine in detail how $\beta\Delta G^*$ depends on the attacker and guard parameters, assuming that we always choose the optimal concentrations given by Eqs. (19) and (20).

Equations (8) and (10) can be used to write two equivalent equations for $\beta\Delta G^*$ by invoking the optimization condition found

in Eq. (16). These are $(\beta\Delta G^*)_1 = \beta G_{\text{attacker}}(N_R') - \beta G_{\text{guard}}(N_R')$ and $(\beta\Delta G^*)_2 = \beta G_{\text{guard}}(N_R'') - \beta G_{\text{attacker}}(N_R'')$. Given that $[(\beta\Delta G^*)_1 + (\beta\Delta G^*)_2]/2 = \beta\Delta G^*$ by definition, then we arrive at

$$\beta\Delta G^* = \frac{N_L}{2} \ln\left(\frac{q_L(c_R'')}{q_L(c_R')} \right) - C_{\text{guard}}^* \left(\frac{N_A a^2 (c_R'' - c_R')}{2} \right). \qquad (25)$$

The factor of Avogadro's number N_A is necessary in the second term, in order to properly convert the surface receptor molarities c_R' and c_R'' into particle counts. In terms of experimental units, the guard design parameter $C_{\text{guard}} = \ln\left(1 + [Gu] K_{eq}^{\text{guard}}\right)$; this is numerically identical to the statistical-mechanical definition in Eq. (9). For further discussion on this equivalence, refer back to Eq. (C14) in Appendix C.

Equation (25) has two distinct terms. The first is a positive (unfavorable) contribution that depends on the attacker design parameters K_{eq}^{attacker} [in the $q_L(c_R)$ factors] and N_L (in the prefactor). The second term is a negative (favorable) contribution that depends on the guard design C_{guard}.

These two terms can be analyzed in the context of Fig. 3(a). Clearly, the only way to *increase* the size of the free energy gap $\beta\Delta G^*$ is to make the slope of the blue (guard) free energy curve more negative. This corresponds to choosing a larger C_{guard} (by choosing either a larger guard concentration or larger binding constant K_{eq}^{guard}). Doing so increases the potential effectiveness ϕ of the recipe in Eq. (17) and also the tolerance to attacker concentration variations around the optimum value.

The attackers, on the other hand, have a less obvious influence on the size of the gap. For extremely weak-binding ligands, then the ratio $q_L(c_R'')/q_L(c_R')$ in Eq. (25) approaches unity, causing that term to vanish to zero so that $\beta\Delta G^*$ is more negative. However, this limit is not experimentally realistic. On the other hand, making the ligands stronger-binding saturates the ratio $(q_L(c_R'')/q_L(c_R')) \to (c_R''/c_R')$ as noted previously. It is then the number of ligands N_L on the attacker that serves to multiply the logarithm of this ratio in Eq. (25), suggesting that attackers with more ligands lead to a potentially less effective and less tolerant design. We return to this point shortly in more quantitative terms.

A beneficial side-effect of Eq. (25) is that the targeting effectiveness ϕ is not particularly sensitive to attacker concentration variations around the optimal value given by Eq. (19). This can be seen in the numerical examples in Fig. 5 (upper panel). The attacker concentration only shifts the binding free energy of the attackers by a constant logarithmic factor $\ln[At]$ [appearing as $\ln z_{\text{attacker}}$ in Eq. (10)]. For example, shifting the attacker binding free energy (red) curve in Fig. 3(a) downward by, say, $2kT$, corresponds to increasing the attacker particle concentration by a large factor of $e^2 \approx 7.4$. However, this will have little impact on the effectiveness ϕ since increasing $\beta\Delta G(N_R')$ by $-2kT$ and $\beta\Delta G(N_R')$ by $2kT$ leads both to still be very near $\beta\Delta G^*$ (assuming that $\beta\Delta G^*$ is already somewhat large and negative). Results in the upper panel of Fig. 5 illustrate this point nicely. Varying the attacker molar concentration by a factor of 10^2 (i.e., from the red to the green dataset in that figure) only corresponds to a change in effectiveness from $\phi^* = 0.95$ to 0.8.
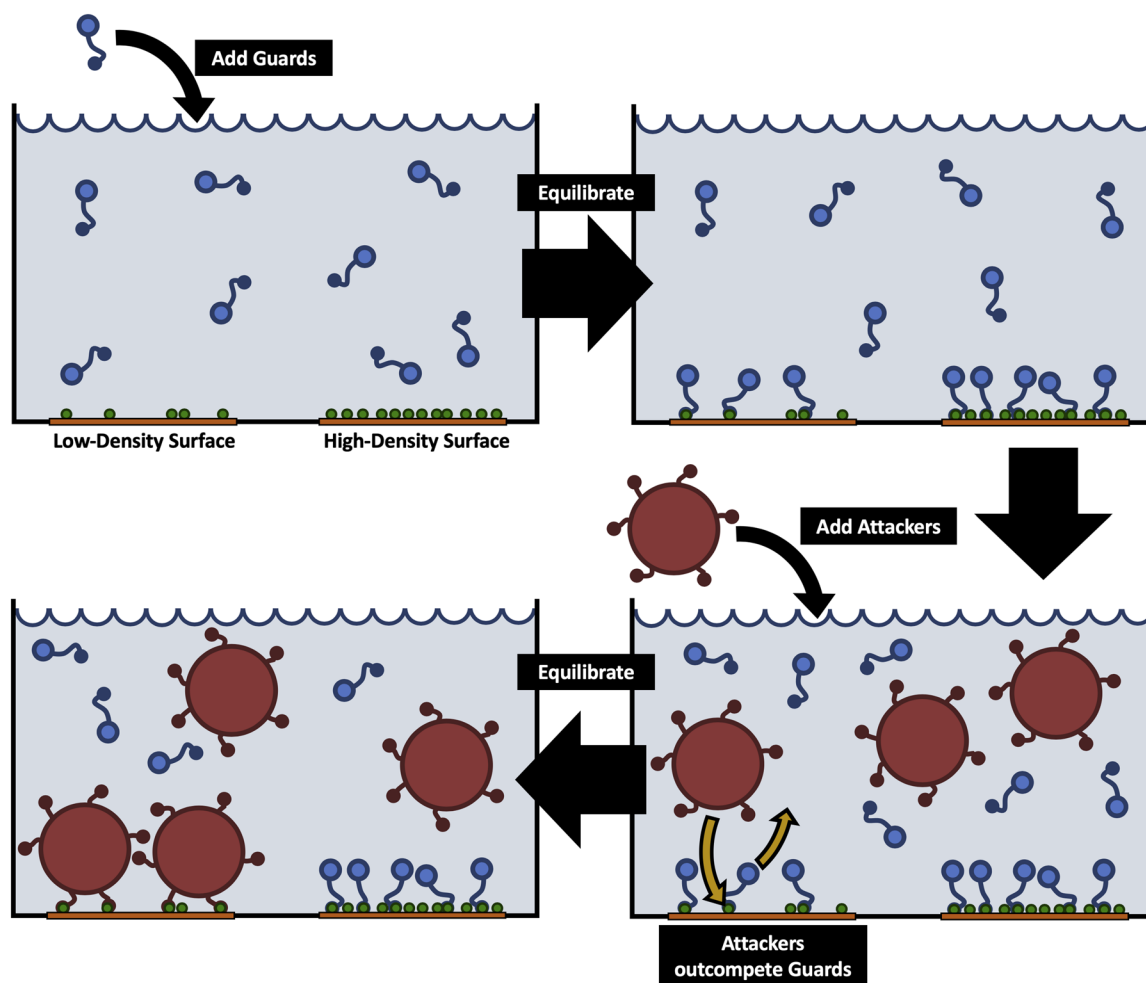
FIG. 6. Graphical depiction of a kinetically facile approach to reaching Attacker and Guard equilibrium in a hypothetical solution containing a low- and high-receptor-density surface. Adding guards (upper left) to the solution and then equilibrating leads guards to bind to receptors on both surfaces (upper right). Attackers are then titrated into the solution (lower right), and they outcompete for binding on the low-density surface due to their more favorable binding free energy at that receptor density (lower left).

By contrast, the targeting effectiveness is more sensitive to variations in guard concentration $[Gu]$ as this factor goes into the *slope* of the guard binding free energy in Fig. 3(a) (blue curve) as z_{guard} in Eq. (8). For example, in the lower panel of Fig. 5, changing the guard concentration only by a factor of two (i.e., going from the red curve to the green curve) corresponds to the same change in effectiveness from $\phi^* = 0.95$ to 0.8 enacted by changing the attacker concentration by a factor of 100.

The number of receptors N_R' and N_R'' per lattice site on the two surfaces also plays a role in $\beta\Delta G^*$. In particular, as the disparity between N_R' and N_R'' grows larger, an attacker design with weaker binding or lower concentration can be employed in order to obtain a given targeting effectiveness ϕ^*. Numerical examples of this are given in Fig. 7, showing how $[At]^*$ varies as the receptor concentration σ_R' on the low-density surface grows closer to that on the high-density surface (having $\sigma_R'' a^2 = 10$).

A qualitatively similar trend is observed for the selections of ligand/receptor binding constant K_{eq}^{attacker} and targeting effectiveness $\phi^* = 0.95$ and 0.5. As σ_R' grows closer to σ_R'', the attacker and guard recipe demands a larger attacker binding constant or bulk concentration. When lower targeting effectiveness is sought, then lower values for these two parameters are called for. Figure 7 also shows how the optimal guard concentration $[Gu]^*$ varies comparatively little with σ_R' at fixed σ_R'', assuming a moderate-binding $1/K_{eq}^{\text{guard}} = 10$ μM.

A somewhat counter-intuitive observation in Eq. (25) is that increasing the number of ligands N_L on the attackers actually leads to a *smaller* free energy gap. Looking at Fig. 3(a), a larger $\beta\Delta G^*$ is obtained when the attacker free energy (red curve) approaches behaving like a horizontal line between N_R' and N_R''. However, increasing N_L causes the attacker free energy to exhibit a more negative gradient for larger values of N_R, as demonstrated in Fig. 1(b).
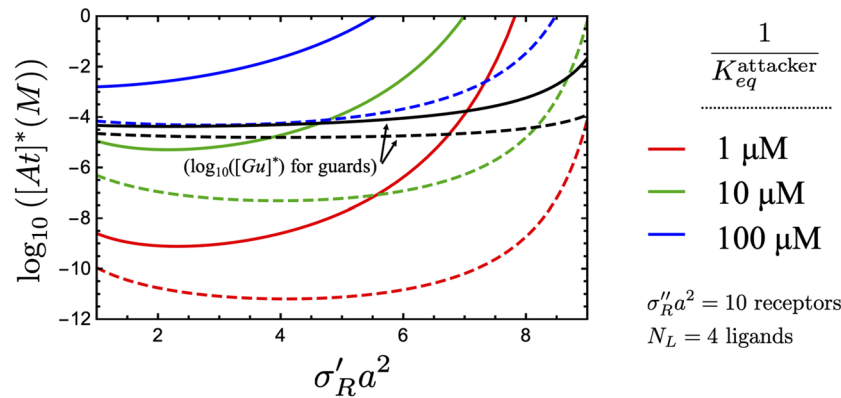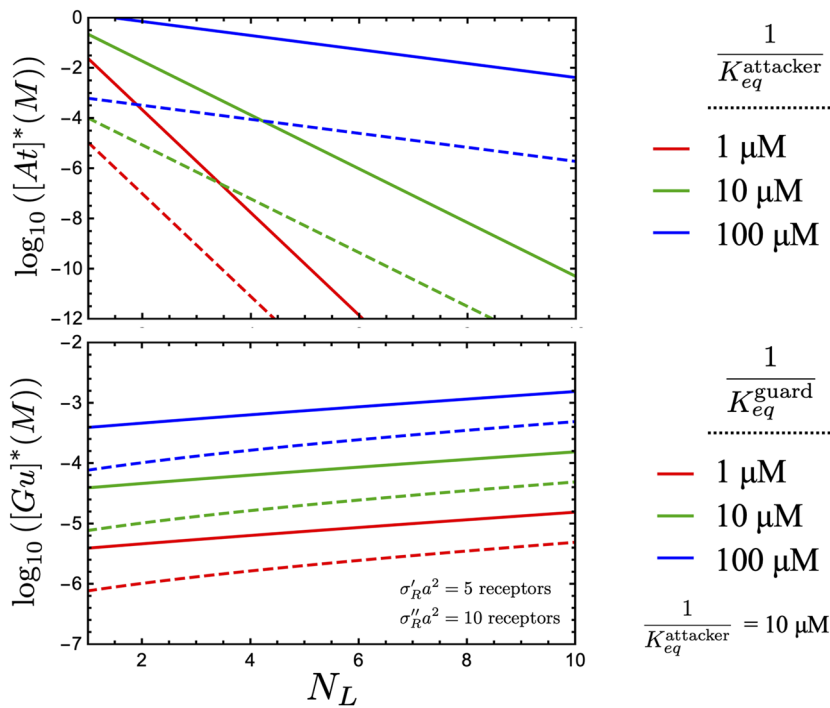
FIG. 7. Logarithm of the optimal attacker concentration $[At]^*$ as a function of the number of receptors per attacker footprint, $\sigma_R' a^2$, on the low-density surface. The high-density surface is fixed at $\sigma_R'' a^2 = 10$. Attackers have $N_L = 4$ ligands, diameter $a = 50$ nm, and an equilibrium binding height $h_{bind} = 15$ nm. Results for three choices of ligand/receptor dissociation constants $1/K_{eq}^{attacker}$ in the micromolar range are given (blue, green, and red). Black curves are the logarithm of the optimal guard concentration $[Gu]^*$ vs $\sigma_R' a^2$ when their dissociation constant is $1/K_{eq}^{guard} = 10\ \mu M$ and when attackers also have $1/K_{eq}^{attacker} = 10\ \mu M$. For all datasets, solid lines are for targeting effectiveness $\phi^* = 0.95$, and dashed lines are for 0.5.

Larger attacker valence therefore limits the targeting effectiveness of the attacker/guard recipe, again in contrast to standard multivalent reasoning. On the other hand, choosing small N_L has kinetic consequences as attackers with fewer ligands will exhibit a slower rate of surface adsorption.

Figure 8 presents numerical results for how the optimal concentrations $[At]^*$ and $[Gu]^*$ vary with N_L. Examining Eq. (19) and taking the strong-ligand limit where $(q_L(c_R'')/q_L(c_R')) \rightarrow (c_R''/c_R')$ yields a scaling of

$$\ln[At]^* \propto -N_L \ln\left(\frac{K_{eq}^{attacker}\sqrt{c_R' c_R''}}{h_{bind}}\right) + \frac{N_L}{2}\left(\frac{c_R'' + c_R'}{c_R'' - c_R'}\right)\ln\left(\frac{c_R''}{c_R'}\right). \tag{26}$$

FIG. 8. Logarithm of the optimal attacker (top panel) and guard (bottom panel) concentrations as a function of the number of ligands N_L on the attackers. Attackers have diameter $a = 50$ nm and an equilibrium binding height $h_{bind} = 15$ nm. The low- and high-receptor-density surfaces have $\sigma_R' a^2 = 5$ and $\sigma_R'' a^2 = 10$ receptors per attacker footprint a^2, respectively. Results are presented for three choices of micromolar-range dissociation constants $1/K_{eq}^{attacker}$ and $1/K_{eq}^{guard}$ (red, green, and blue) and for two choices of targeting effectiveness ϕ^*: 0.95 (solid) and 0.5 (dashed). For guard calculations in lower panel, $1/K_{eq}^{attacker} = 10\ \mu M$.

The first term in this expression tends to dominate in Fig. 8 (upper panel), giving rise to the linear trends. As intuition would suggest, adding more ligands with the same binding strength K_{eq}^{attacker} to the attackers leads to a lower optimal solution concentration $[At]^*$. Increasing the intended targeting effectiveness ϕ^* just causes a uniform upward shift in the optimal concentration $[At]^*$. However, the optimal guard concentration $[Gu]^*$ changes little with N_L in Fig. 8 (lower panel). In the strong-ligand limit for the *attackers*, the optimal *guard* concentration in Eq. (20) scales as

$$\ln[Gu]^* \propto \frac{N_L}{a^2(c_R'' - c_R')} \ln\left(\frac{c_R''}{c_R'}\right). \tag{27}$$

This lacks the strong binding constant dependence like the attackers.

D. Complications to effective targeting and to the present theory

It has been assumed that the attackers are large enough when bound so as to sterically exclude all receptors in their surface "footprint" of area a^2 from binding to any guard particles. This might be difficult to achieve in the experiment; guard particles might slip beneath the bound attackers to occupy some of the receptors, thereby reducing the statistical average number of attackers bound on the target low-density surface. The quantitative result in Fig. 3(b) would be a lowering of the red curve and a raising of the blue curve in the low-receptor range (i.e., on the surface(s) where attackers dominate). The overall targeting effectiveness ϕ by Eq. (14)] will be accordingly reduced. In general, the more easily that guards can penetrate beneath bound attackers, the lower the resulting effectiveness of the strategy will be. One possibility is to add bulky groups to the guards so that they are less likely to invade attacker-occupied surface territory.

In addition to ligand-receptor interactions, it was noted in Eq. (2) that multivalent particles can also have a nonspecific interaction free energy βG_{NS} with their target surface. However, as demonstrated in Eq. (5), any such contribution just becomes an additive factor in the multivalent binding free energy. Therefore, the only influence of βG_{NS} is to shift the attacker binding free energy [e.g., red curve, Fig. 3(a)] by a constant factor. This will quantitatively shift the predicted $[At]^*$ upward if βG_{NS} is positive or downward if βG_{NS} is negative. However, it will not affect the possibility of selectively targeting the low-density surface.

Early in our discussion, we made the approximation that the attacker binding free energy follows the form of Eq. (5) so that we could proceed analytically. This expression *over-estimates* the binding free energy for a multivalent particle/surface interaction in which the number of receptors within binding range of the particle is near or less than the number of ligands on the particle, particularly if the ligands are strong-binding. However, the molecular recipe arising out of our discussion is more selective when the multivalent attackers have *few* ligands (as opposed to many). In cases where the number of receptors within the binding range of the attacker is small relative to the number of ligands on the particle, then the true binding free energy will be less favorable (less negative) than predicted by Eq. (5). The predicted optimal attacker concentration $[At]^*$ will therefore be underestimated by Eq. (19) for the system at

hand. This quantitative difference does not prevent selective targeting of the low-receptor-density surface nor does it qualitatively alter the targeting recipe presented here.

V. CONCLUSIONS AND EXPERIMENTAL IMPLEMENTATION

Multivalent particles cannot, on their own, selectively bind to a surface with a low density of receptors while not binding to one with a higher density of the same receptors in the same system. To address this challenge, we have defined a strategy using competitive binding of *two* particle species. The first species, called "guards," are monovalent particles that bind equally well to any receptor on any surface. A second species, called "attackers," is multivalent particles designed to outcompete the guards for binding on the low-receptor-density surface but not on the surface with higher receptor density. At equilibrium, therefore, the attackers occupy the low-density surface, while the guards occupy the high-density surface.

An optimal targeting recipe and several guidelines have been derived and deduced in our discussion that can be directly employed in the experiment. These are now summarized as follows:

- The guards are small (receptor-sized) monovalent particles, with a receptor association constant of K_{eq}^{guard} and a solution concentration of $[Gu]$. These particles are added *first* in the system and allowed to bind and equilibrate on both receptor surfaces.
- The attackers are larger multivalent particles at a solution concentration of $[At]$, each having N_L ligands that can reach multiple receptors when the host multivalent particle is at a given fixed surface position. Their ligand-receptor association constant is K_{eq}^{attacker}. These particles are added *second* into the system. The attackers will, by design, outcompete the guards for binding on the low-receptor-density surface but not the high-receptor-density surface.
- Equations (19) and (20) define the optimal attacker and guard solution concentrations, given their chosen individual ligand-receptor binding constants K_{eq}^{attacker} and K_{eq}^{guard}, the attacker valence N_L, and the surface receptor molarities c_R' and c_R'' on the low- and high-receptor-density surfaces, respectively. These equations are employed by inputting a desired "targeting effectiveness" parameter ϕ^* between 1 (perfect attacker binding selectivity for the low-receptor-density surface) and 0 (no binding selectivity).
- More effective targeting (ϕ^* approaching 1) requires *stronger-binding* attackers and guards, at *larger* solution concentrations. This is contrary to standard multivalent targeting. However, stronger-binding guards also lead to longer equilibration time on the low-density surface when the attackers are added. The larger the difference between the receptor densities on the two surfaces, the weaker the attacker, and guard binding strengths/concentrations can be in order to achieve a given targeting effectiveness.
- More effective targeting occurs when the number of ligands on the attackers is small. However, multivalent particles with fewer ligands will have a longer time scale for forming bonds with surface receptors.

The best approach is therefore to use strong-binding guards that still have a reasonable unbinding time scale, and comparably strong-binding attackers that have several ligands. The best design can be identified by exploring a range of targeting effectiveness values ϕ^* in Eqs. (19) and (20) to find arrive at a guard/attacker motif that is kinetically and thermodynamically suitable. After putting the guards into the system at a concentration of $[Gu]^*$ based on Eq. (20), attackers can be titrated in until they are near a concentration of $[At]^*$ given by Eq. (19). Values of $[At] > [At]^*$ may work equally well, in order to overcome additional nonspecific binding free energy contributions between the attackers and the target surface; the effectiveness of targeting does not depend strongly on $[At]$ above $[At]^*$.

A prime application for this targeting strategy is to selectively image cell surfaces, or regions of cell surfaces, with locally low receptor density compared to other cell surfaces in the same system *in vitro*. This could be done by attaching a fluorescent probe to the attackers, but not the guards. Examples of promising structures that could act as attackers include ligand-coated nanoparticles, functionalized vesicles, DNA origami/dendrimer constructs, star polymers, or modified viruses. The binding equilibrium constants of the guards and attackers could be tuned by a DNA approach, e.g., like in DNA-PAINT.[73] The attacker and guard recipe could also be used to selectively sequester or aggregate a population of nanoscopic entities in solution with a low receptor density, with attackers acting as the aggregation/sequestration agent.

ACKNOWLEDGMENTS

APPENDIX A: MULTIVALENT ATTACKER AND MONOVALENT GUARD BINDING PROBABILITIES

The partition function for a surface lattice site is given, based on Eqs. (8) and (10), as

$$Q(N_R) = \left(1 + z_{\text{guard}}e^{-\beta f_{\text{guard}}}\right)^{N_R} + z_{\text{attacker}}\left(1 + N_R e^{-\beta f_{\text{attacker}}}\right)^{N_L}$$
$$= Q_{\text{guard}}(N_R) + Q_{\text{attacker}}(N_R). \tag{A1}$$

The first term in $Q(N_R)$ represents all possible guard binding states, and the second term is for all attacker binding states. The state in which the lattice site has neither an attacker nor any guards bound, having a weight of unity, is included in the first term of $Q(N_R)$. This partition function also includes the state in which an attacker is within the surface lattice site but has no ligands bound to receptors.

The probability that a surface lattice site is occupied by an attacker is just the ratio of $Q_{\text{attacker}}(N_R)$ to $Q(N_R)$ for a given number of receptors N_R in the lattice site

$$P_b^{\text{attacker}}(N_R) = \frac{Q_{\text{attacker}}(N_R)}{Q_{\text{attacker}}(N_R) + Q_{\text{guard}}(N_R)}$$
$$= \frac{e^{-\beta G_{\text{attacker}}(N_R)}}{e^{-\beta G_{\text{attacker}}(N_R)} + e^{-\beta G_{\text{guard}}(N_R)}}. \tag{A2}$$

By defining the quantity

$$\beta \Delta G(N_R) = \beta G_{\text{attacker}}(N_R) - \beta G_{\text{guard}}(N_R), \tag{A3}$$

then $P_b^{\text{attacker}}(N_R)$ reduces to the simple form

$$P_b^{\text{attacker}}(N_R) = \frac{e^{-\beta \Delta G(N_R)}}{1 + e^{-\beta \Delta G(N_R)}}, \tag{A4}$$

as shown in Eq. (11).

The probability that a single receptor on the surface is occupied by a monovalent guard is found by

$$P_b^{\text{guard}}(N_R) = \frac{1}{N_R}\frac{d \ln Q(N_R)}{d\beta \mu_{\text{guard}}}, \tag{A5}$$

where $\beta \mu_{\text{guard}} = \ln z_{\text{guard}}$ is the chemical potential of the guards in solution. This leads to

$$P_b^{\text{guard}}(N_R) = \left(\frac{z_{\text{guard}}e^{-\beta f_{\text{guard}}}}{1 + z_{\text{guard}}e^{-\beta f_{\text{guard}}}}\right)\left(1 - P_b^{\text{attacker}}(N_R)\right), \tag{A6}$$

shown as Eq. (13) in the main text.

APPENDIX B: OPTIMAL TARGETING EFFECTIVENESS AND TOLERANCE

The targeting effectiveness is defined as

$$\phi \equiv P_b^{\text{attacker}}(N_R') - P_b^{\text{attacker}}(N_R''), \tag{B1}$$

where

$$P_b^{\text{attacker}}(N_R) = \frac{e^{-\beta \Delta G(N_R)}}{1 + e^{-\beta \Delta G(N_R)}}. \tag{B2}$$

The free energy difference $\beta \Delta G(N_R)$ is

$$\beta \Delta G(N_R) = \beta G_{\text{attacker}}(N_R) - \beta G_{\text{guard}}(N_R)$$
$$= -N_L \ln[q_L(N_R)] - \ln z_{\text{attacker}} + N_R C_{\text{guard}}, \tag{B3}$$

where

$$q_L(N_R) = \left(1 + N_R e^{-\beta f_{\text{attacker}}}\right) \tag{B4}$$

is the partition function for one ligand on the attacker given N_R possible receptors to attach to nearby.

Choosing the parameter C_{guard} effectively sets the guard binding free energy and fugacity in solution. In the experiment, it is also reasonable to assert that the number of ligands N_L and ligand/receptor binding free energy f_{attacker} have been set based on the chemical design of the attackers. Thus, the remaining free variable to optimize is the attacker fugacity z_{attacker}—that is, the

solution concentration $[At]$ of attackers that maximizes the targeting effectiveness ϕ.

The attacker fugacity yielding the largest possible effectiveness ϕ is obtained where

$$\frac{d\phi}{d\ln z_{\text{attacker}}} = \frac{d(\beta\Delta G(N_R''))}{d\ln z_{\text{attacker}}}\frac{e^{-\beta\Delta G(N_R'')}}{\left(1 + e^{-\beta\Delta G(N_R'')}\right)^2}$$
$$- \frac{d(\beta\Delta G(N_R'))}{d\ln z_{\text{attacker}}}\frac{e^{-\beta\Delta G(N_R')}}{\left(1 + e^{-\beta\Delta G(N_R')}\right)^2} = 0. \qquad (B5)$$

Inspecting Eq. (B3), the two derivatives of $\beta\Delta G(N_R)$ with respect to $\ln z_{\text{attacker}}$ are identical and independent of N_R. Thus, Eq. (B5) is zero when either $\beta\Delta G(N_R') = \beta\Delta G(N_R'')$ or $\beta\Delta G(N_R') = -\beta\Delta G(N_R'')$. The first solution yields an effectiveness of zero via Eq. (B1), which is obviously not the solution we want. The second solution,

$$\beta\Delta G(N_R') = -\beta\Delta G(N_R'') \equiv \beta\Delta G^*, \qquad (B6)$$

inserted into Eq. (B1) yields the optimal effectiveness

$$\phi^* \equiv \frac{e^{-\beta\Delta G^*} - 1}{e^{-\beta\Delta G^*} + 1}. \qquad (B7)$$

This is given as Eq. (17) in the main text.

To ensure that $\beta\Delta G(N_R') = -\beta\Delta G(N_R'')$ corresponds to a maximum in Eq. (B1), we check the sign of the second derivative of the function ϕ with respect to $\ln z_{\text{attacker}}$ at $\beta\Delta G(N_R') = -\beta\Delta G(N_R'') = \beta\Delta G^*$,

$$\frac{d^2\phi}{[d\ln z_{\text{attacker}}]^2} = 2e^{-\beta\Delta G^*}\left[\frac{1 - e^{-\beta\Delta G^*}}{(1 + e^{-\beta\Delta G^*})^3}\right]. \qquad (B8)$$

The second derivative is always negative, and therefore the condition $\beta\Delta G(N_R') = -\beta\Delta G(N_R'')$ always corresponds to a maximum, as long as $\beta\Delta G^* < 0$. This is true for *any* design which selectively targets the attackers to the low-receptor-density surface. When $\beta\Delta G^* \ll 0$, then

$$-\left(\frac{d^2\phi}{[d\ln z_{\text{attacker}}]^2}\right)^{-1} \approx \frac{1}{2}e^{-\beta\Delta G^*} \equiv \text{Design Tolerance}. \qquad (B9)$$

This illustrates how designing the attackers and guards to have a more negative $\beta\Delta G^*$ causes the design to be more robust/tolerant to variations in molecular construction and concentration.

APPENDIX C: OPTIMAL ATTACKER AND GUARD DESIGN PARAMETERS

The binding free energies for guards $[\beta G_{\text{guard}}(N_R)]$ and attackers $[\beta G_{\text{attacker}}(N_R)]$ are given by Eqs. (8) and (10), respectively. Guards are defined by the choice of the parameter C_{guard}, and attackers are given a predefined valence N_L and ligand/receptor binding free energy f_{attacker}. In Appendix B, we showed that the choice of attacker fugacity z_{attacker} that maximizes the effectiveness ϕ corresponds to when $\beta G_{\text{attacker}}(N_R') - \beta G_{\text{guard}}(N_R') = \beta G_{\text{guard}}(N_R'') - \beta G_{\text{attacker}}(N_R'')$. With Eqs. (8) and (10), this condition yields the equation

$$\ln z_{\text{attacker}} = \frac{(N_R' + N_R'')}{2}C_{\text{guard}} - \frac{N_L}{2}\ln\left[q_L(N_R')q_L(N_R'')\right], \qquad (C1)$$

where $q_L(N_R)$ is given by Eq. (B4). Next, the relation $\beta\Delta G^* = -\ln\left(\frac{1+\phi^*}{1-\phi^*}\right) = \beta G_{\text{attacker}}(N_R') - \beta G_{\text{guard}}(N_R')$ from Eq. (17) allows us to write another equation with Eqs. (8) and (10),

$$-\ln\left(\frac{1+\phi^*}{1-\phi^*}\right) = -N_L\ln\left[q_L(N_R')\right] - \ln z_{\text{attacker}} + N_R'C_{\text{guard}}. \qquad (C2)$$

Isolating $\ln z_{\text{attacker}}$ in this equation and then putting it back into Eq. (C1) allows us to solve for the optimal C_{guard} given a choice of targeting effectiveness ϕ^*,

$$C_{\text{guard}}^* = \left(\frac{2}{N_R'' - N_R'}\right)\ln\left[\left(\frac{q_L(N_R'')}{q_L(N_R')}\right)^{\frac{N_L}{2}}\left(\frac{1+\phi^*}{1-\phi^*}\right)\right]. \qquad (C3)$$

Putting this back into Eq. (C1) then yields

$$\ln z_{\text{attacker}}^* = \left(\frac{N_R'' + N_R'}{N_R'' - N_R'}\right)\ln\left[\left(\frac{q_L(N_R'')}{q_L(N_R')}\right)^{\frac{N_L}{2}}\left(\frac{1+\phi^*}{1-\phi^*}\right)\right]$$
$$- \frac{N_L}{2}\ln\left(q_L(N_R')q_L(N_R'')\right). \qquad (C4)$$

Equations (C3) and (C4) can be readily converted into a chemical equilibrium notation. First, all instances of N_R' and N_R'' can be identically expressed in terms of average surface receptor densities σ_R' and σ_R''. (Recall that the receptor density σ_R is related to N_R by $N_R = a^2\sigma_R$; the length a is the diameter of one attacker particle, and a^2 therefore measures the area over which the particle can bind to receptors on the surface.) This substitution leads to

$$C_{\text{guard}}^* = \left[\frac{2}{a^2(\sigma_R'' - \sigma_R')}\right]\ln\left[\left(\frac{q_L(\sigma_R'')}{q_L(\sigma_R')}\right)^{\frac{N_L}{2}}\left(\frac{1+\phi^*}{1-\phi^*}\right)\right], \qquad (C5)$$

$$\ln z_{\text{attacker}}^* = \left(\frac{\sigma_R'' + \sigma_R'}{\sigma_R'' - \sigma_R'}\right)\ln\left[\left(\frac{q_L(\sigma_R'')}{q_L(\sigma_R')}\right)^{\frac{N_L}{2}}\left(\frac{1+\phi^*}{1-\phi^*}\right)\right]$$
$$- \frac{N_L}{2}\ln\left(q_L(\sigma_R')q_L(\sigma_R'')\right), \qquad (C6)$$

where

$$q_L(\sigma_R) = \left(1 + a^2\sigma_R e^{-\beta f_{\text{attacker}}}\right). \qquad (C7)$$

The remaining challenge is to express the following quantities in terms of the receptor binding constant K_{eq}^{attacker} for ligands on the attacker, the guard binding constant K_{eq}^{guard}, and guard/attacker molar concentrations $[Gu]$ and $[At]$,

$$C_{\text{guard}}^* = \ln\left(1 + z_{\text{guard}}e^{-\beta f_{\text{guard}}}\right)^*, \qquad (C8)$$

$$\ln z_{\text{attacker}}^* \qquad (C9)$$

$$q_L(\sigma_R) = \left(1 + a^2\sigma_R e^{-\beta f_{\text{attacker}}}\right). \qquad (C10)$$

This process is now described in detail.

Recall that the equilibrium constant K_{eq} for two binding entities "B" and "R," in a hypothetical solution, is defined as

$$K_{eq} = \frac{[BR]}{[B][R]}. \tag{C11}$$

Here, $[BR]$ is the equilibrium concentration of B bound to R, while $[B]$ and $[R]$ are the equilibrium concentrations of unbound B and R. Let us suppose that species R are receptors on a surface, while species B are binders in solution above the surface. If we go to the grand-canonical limit where the number of B particles is far in excess of the number of R particles, then $[B] \approx [B]^\circ$, where $[B]^\circ$ is the (fixed) solution concentration of B regardless of how many are bound to R. This leads to

$$K_{eq} = \frac{1}{[B]^\circ}\left(\frac{[BR]}{[R]}\right) = \frac{1}{[B]^\circ}\left(\frac{N_{R,bound}}{N_{R,free}}\right), \tag{C12}$$

where $N_{R,bound}$ and $N_{R,free}$ are the number of receptors that are bound to B and unbound, respectively. The number of unbound receptors at equilibrium is given by $N_{R,free} = N_R - N_{R,bound}$, where N_R is the total number of receptors on the surface. This is directly related to the equilibrium binding free energy βf of B to R by the statistical mechanical relationship

$$\left(\frac{N_{R,bound}}{N_R - N_{R,bound}}\right) = z([B]^\circ)e^{-\beta f}, \tag{C13}$$

where $z([B]^\circ)$ is the fugacity corresponding to the solution concentration $[B]^\circ$. Bringing the concentration factor $[B]^\circ$ onto the left-hand side of Eq. (C12) yields

$$K_{eq}[B]^\circ = z([B]^\circ)e^{-\beta f}. \tag{C14}$$

This is the direct relationship between the experimental quantity $K_{eq}[B]^\circ$ and the statistical thermodynamic quantity $z([B]^\circ)e^{-\beta f}$.

Using Eq. (C14), we can immediately convert $z_{guard}e^{-\beta f_{guard}}$ in Eq. (C8) into experimental units for the guards

$$z_{guard}e^{-\beta f_{guard}} = [Gu]K_{eq}^{guard}, \tag{C15}$$

where $[Gu]$ is the molar solution concentration of the guards.

Next, the fugacity $z_{attacker}$ of the attackers is related to their molar solution concentration $[At]$ via Eq. (1)

$$z_{attacker} = [At]N_A h_{bind}a^2, \tag{C16}$$

where $h_{bind}a^2$ is the "localization volume" for placing the ligands of the particle in contact with the surface receptors.

Turning lastly to $q_L(\sigma_R)$, the quantity $\sigma_R a^2$ acts as a two-dimensional receptor fugacity and $\exp(-\beta f_{attacker})$ is the binding strength term. Thus, we can again invoke Eq. (C14) to write Eq. (C10) as

$$q_L([R]_{eff}) = \left(1 + [R]_{eff}e^{-\beta f_{attacker}}\right), \tag{C17}$$

where $[R]_{eff}$ is the effective molarity of receptors on the surface, as seen by ligands on bound attackers. The effective molarities on the low- and high-density surfaces are related to the surface (number)

densities σ_R' and σ_R'' via the equilibrium binding distance h_{bind} of the attacker

$$[R]_{eff}' = \frac{\sigma_R'}{N_A h_{bind}} = \frac{c_R'}{h_{bind}}, \tag{C18}$$

$$[R]_{eff}'' = \frac{\sigma_R''}{N_A h_{bind}} = \frac{c_R''}{h_{bind}}. \tag{C19}$$

For notational clarity, the molar surface receptor density $c_R = \sigma_R/N_A$ has been defined, having dimensions of moles of receptors per unit surface area. Re-expressing Eq. (C17) in terms of c_R and h_{bind} yields

$$q_L(c_R) = \left(1 + \frac{c_R K_{eq}^{attacker}}{h_{bind}}\right). \tag{C20}$$

These transformations enable us to write the expressions for the optimal guard design C_{guard}^* [Eq. (C5)] and attacker fugacity $z_{attacker}^*$ [Eq. (C6)] in terms of experimental quantities

$$\ln[At]^* = \left(\frac{c_R'' + c_R'}{c_R'' - c_R'}\right)\ln\left[\left(\frac{q_L(c_R'')}{q_L(c_R')}\right)^{\frac{N_L}{2}}\left(\frac{1+\phi^*}{1-\phi^*}\right)\right]$$
$$- \frac{N_L}{2}\ln\left(q_L(c_R')q_L(c_R'')\right) - \ln\left(N_A h_{bind}a^2\right), \tag{C21}$$

$$\ln\left(1 + [Gu]^* K_{eq}^{guard}\right) = \left[\frac{2}{N_A a^2\left(c_R'' - c_R'\right)}\right]$$
$$\times \ln\left[\left(\frac{q_L(c_R'')}{q_L(c_R')}\right)^{\frac{N_L}{2}}\left(\frac{1+\phi^*}{1-\phi^*}\right)\right], \tag{C22}$$

where $q_L(c_R)$ is calculated by Eq. (C20).

In this form, we have assumed that the ligand/receptor binding constants K_{eq}^{guard} and $K_{eq}^{attacker}$, as well as the number of ligands N_L on the attackers, are set based on the chemical construction of the attackers and guards. Achieving the optimum targeting effectiveness is thus left to tuning of the attacker and guard solution concentrations to the optimal values $[At]^*$ and $[Gu]^*$. The explicit equations for these two quantities are obtained by isolating $[At]^*$ and $[Gu]^*$ in Eqs. (C21) and (C22). This is done to yield Eqs. (19) and (20) in the main text.

REFERENCES

[1] G. Bell, Science **200**, 618 (1978).

[2] G. I. Bell, M. Dembo, and P. Bongrand, Biophys. J. **45**, 1051 (1984).

[3] B. Sulzer and A. S. Perelson, Math. Biosci. **135**, 147 (1996).

[4] J. Huskens, A. Mulder, T. Auletta, C. A. Nijhuis, M. J. W. Ludden, and D. N. Reinhoudt, J. Am. Chem. Soc. **126**, 6784 (2004).

[5] F. J. Martinez-Veracoechea and D. Frenkel, Proc. Natl. Acad. Sci. U. S. A. **108**, 10963 (2011).

[6] P. Varilly, S. Angioletti-Uberti, B. M. Mognetti, and D. Frenkel, J. Chem. Phys. **137**, 094108 (2012).

[7] S. Angioletti-Uberti, P. Varilly, B. M. Mognetti, A. V. Tkachenko, and D. Frenkel, J. Chem. Phys. **138**, 021102 (2013).

[8] F. J. Martinez-Veracoechea and M. E. Leunissen, Soft Matter **9**, 3213 (2013).

[9] C. A. Macken and A. S. Perelson, J. Math. Biol. **14**, 365 (1982).

[10] A. S. Perelson, Math. Biosci. **49**, 87 (1980).

[11] B. Sulzer and A. S. Perelson, Mol. Immunol. **34**, 63 (1997).

[12] W. S. Hlavacek, J. K. Percus, O. E. Percus, A. S. Perelson, and C. Wofsy, Math. Biosci. **176**, 185 (2002).

[13] H.-Y. Chen, Phys. Rev. E **67**, 031919 (2003).

[14] S. Hong, P. R. Leroueil, I. J. Majoros, B. G. Orr, J. R. Baker, Jr., and M. M. Banaszak Holl, Chem. Biol. **14**, 107 (2007).

[15] C. B. Carlson, P. Mowery, R. M. Owen, E. C. Dykhuizen, and L. L. Kiessling, ACS Chem. Biol. **2**, 119 (2007).

[16] S. F. Shimobayashi, B. M. Mognetti, L. Parolini, D. Orsi, P. Cicuta, and L. Di Michele, Phys. Chem. Chem. Phys. **17**, 15615 (2015).

[17] H. Xu and D. E. Shaw, Biophys. J. **110**, 218 (2016).

[18] T. R. Weikl, J. Hu, G.-K. Xu, and R. Lipowsky, Cell Adhes. Migr. **10**, 576 (2016).

[19] T. Curk, J. Dobnikar, and D. Frenkel, Proc. Natl. Acad. Sci. U. S. A. **114**, 7210 (2017).

[20] O. A. Amjad, B. M. Mognetti, P. Cicuta, and L. Di Michele, Langmuir **33**, 1139 (2017).

[21] S. Angioletti-Uberti, npj Comput. Mater. **3**, 48 (2017).

[22] L. Di Michele, P. K. Jana, and B. M. Mognetti, Phys. Rev. E **98**, 032406 (2018).

[23] M. Mammen, S. K. Choi, and G. M. Whitesides, Angew. Chem., Int. Ed. **37**, 2754 (1998).

[24] L. L. Kiessling and J. C. Grim, Chem. Soc. Rev. **42**, 4476 (2013).

[25] C. T. Varner, T. Rosen, J. T. Martin, and R. S. Kane, Biomacromolecules **16**, 43 (2015).

[26] S. Liese and R. R. Netz, ACS Nano **12**, 4140 (2018).

[27] S. Shao, Q. Zhou, J. Si, J. Tang, X. Liu, M. Wang, J. Gao, K. Wang, R. Xu, and Y. Shen, Nat. Biomed. Eng. **1**, 745 (2017).

[28] S. Wilhelm, A. J. Tavares, Q. Dai, S. Ohta, J. Audet, H. F. Dvorak, and W. C. W. Chan, Nat. Rev. Mater. **1**, 16014 (2016).

[29] K. Ren and R. N. Zare, ACS Nano **6**, 4314 (2012).

[30] G. V. Dubacheva, T. Curk, R. Auzély-Velty, D. Frenkel, and R. P. Richter, Proc. Natl. Acad. Sci. U. S. A. **112**, 5579 (2015).

[31] N. A. Licata and A. V. Tkachenko, Phys. Rev. Lett. **100**, 158102 (2008).

[32] C. S. Mahon and D. A. Fulton, Nat. Chem. **6**, 665 (2014).

[33] R. de laRica, R. M. Fratila, A. Szarpak, J. Huskens, and A. H. Velders, Angew. Chem., Int. Ed. **50**, 5704 (2011).

[34] N. B. Tito and D. Frenkel, Macromolecules **47**, 7496 (2014).

[35] J. Vonnemann, S. Liese, C. Kuehne, K. Ludwig, J. Dernedde, C. Böttcher, R. R. Netz, and R. Haag, J. Am. Chem. Soc. **137**, 2572 (2015).

[36] B. D. Myers, Q.-Y. Lin, H. Wu, E. Luijten, C. A. Mirkin, and V. P. Dravid, ACS Nano **10**, 5679 (2016).

[37] K. Ren, N. Banaei, and R. N. Zare, ACS Nano **7**, 6031 (2013).

[38] S. Mura, J. Nicolas, and P. Couvreur, Nat. Mater. **12**, 991 (2013).

[39] G. V. Dubacheva, T. Curk, B. M. Mognetti, R. Auzély-Velty, D. Frenkel, and R. P. Richter, J. Am. Chem. Soc. **136**, 1722 (2014).

[40] M. R. Caplan and E. V. Rosca, Ann. Biomed. Eng. **33**, 1113 (2005).

[41] M. K. Robinson, K. M. Hodge, E. Horak, Å. L. Sundberg, M. Russeva, C. C. Shaller, M. von Mehren, I. Shcaveleva, H. H. Simmons, J. D. Marks, and G. P. Adams, Br. J. Cancer **99**, 1415 (2008).

[42] L. Zitvogel and G. Kroemer, OncoImmunology **1**, 1223 (2014).

[43] K.-H. Roh, B. F. Lillemeier, F. Wang, and M. M. Davis, Proc. Natl. Acad. Sci. U. S. A. **112**, E1604 (2015).

[44] M. McKenzie, S. M. Ha, A. Rammohan, R. Radhakrishnan, and N. Ramakrishnan, Biophys. J. **114**, 1830 (2018).

[45] C. A. Mirkin, R. L. Letsinger, R. C. Mucic, and J. J. Storhoff, Nature **382**, 607 (1996).

[46] P. L. Biancaniello, A. J. Kim, and J. C. Crocker, Phys. Rev. Lett. **94**, 058302 (2005).

[47] W. B. Rogers and J. C. Crocker, Proc. Natl. Acad. Sci. U. S. A. **108**, 15687 (2011).

[48] S. Angioletti-Uberti, Nat. Mater. **11**, 518 (2012).

[49] K.-T. Wu, L. Feng, R. Sha, R. Dreyfus, A. Y. Grosberg, N. C. Seeman, and P. M. Chaikin, Phys. Rev. E **88**, 022304 (2013).

[50] C. Stoffelen, J. Voskuhl, P. Jonkheijm, and J. Huskens, Angew. Chem., Int. Ed. **53**, 3400 (2014).

[51] R. Mejia-Ariza and J. Huskens, J. Mater. Chem. B **2**, 210 (2014).

[52] S. Angioletti-Uberti, P. Varilly, B. M. Mognetti, and D. Frenkel, Phys. Rev. Lett. **113**, 128303 (2014).

[53] Q. Li, D. G. Barrett, P. B. Messersmith, and N. Holten-Andersen, ACS Nano **10**, 1317 (2015).

[54] Y. Wang, Y. Wang, X. Zheng, E. Ducrot, J. S. Yodh, M. Weck, and D. J. Pine, Nat. Commun. **6**, 7253 (2015).

[55] T. Curk, U. Bren, and J. Dobnikar, Mol. Phys. **116**, 3392 (2018).

[56] B. Srinivasan, T. Vo, Y. Zhang, O. Gang, S. Kumar, and V. Venkatasubramanian, Proc. Natl. Acad. Sci. U. S. A. **110**, 18431 (2013).

[57] S. C. Grindy, M. Lenz, and N. Holten-Andersen, Macromolecules **49**, 8306 (2016).

[58] S. J. Bachmann, J. Kotar, L. Parolini, A. Šarić, P. Cicuta, L. Di Michele, and B. M. Mognetti, Soft Matter **12**, 7804 (2016).

[59] A. C. Newton, J. Groenewold, W. K. Kegel, and P. G. Bolhuis, Proc. Natl. Acad. Sci. U. S. A. **112**, 15308 (2015).

[60] P. E. Theodorakis, N. G. Fytas, G. Kahl, and C. Dellago, Condens. Matter Phys. **18**, 22801 (2015).

[61] S. A. J. van der Meulen, G. Helms, and M. Dogterom, J. Phys.: Condens. Matter **27**, 233101 (2015).

[62] A. C. Newton, J. Groenewold, W. K. Kegel, and P. G. Bolhuis, J. Chem. Phys. **146**, 234901 (2017).

[63] S. Angioletti-Uberti, B. M. Mognetti, and D. Frenkel, Phys. Chem. Chem. Phys. **18**, 6373 (2016).

[64] B. L. Mbanga, B. V. S. Iyer, V. V. Yashin, and A. C. Balazs, Macromolecules **49**, 1353 (2016).

[65] C. Stoffelen and J. Huskens, Nanoscale **7**, 7915 (2015).

[66] L. Di Michele, S. J. Bachmann, L. Parolini, and B. M. Mognetti, J. Chem. Phys. **144**, 161104 (2016).

[67] Y. Zhang, A. McMullen, L.-L. Pontani, X. He, R. Sha, N. C. Seeman, J. Brujic, and P. M. Chaikin, Nat. Commun. **8**, 21 (2017).

[68] J. D. Halverson and A. V. Tkachenko, J. Chem. Phys. **144**, 094903 (2016).

[69] S. J. Bachmann, M. Petitzon, and B. M. Mognetti, Soft Matter **12**, 9585 (2016).

[70] A. Vijaykumar, P. R. ten Wolde, and P. G. Bolhuis, Mol. Phys. **116**, 3042 (2018).

[71] N. B. Tito, S. Angioletti-Uberti, and D. Frenkel, J. Chem. Phys. **144**, 161101 (2016).

[72] N. B. Tito and D. Frenkel, Eur. Phys. J.: Spec. Top. **225**, 1673 (2016).

[73] P. Delcanale, B. Miret-Ontiveros, M. Arista-Romero, S. Pujals, and L. Albertazzi, ACS Nano **12**, 7629 (2018).

[74] G. V. Dubacheva, T. Curk, D. Frenkel, and R. P. Richter, J. Am. Chem. Soc. **141**, 2577 (2019).